Toward the Recognition of Unaccounted for Flange Local Buckling and Tension Flange Yielding Resistances in the ANSI/AISC 360 Specification

Oğuzhan Toğay[1] and Donald W. White[2]

Abstract
The Flange Local Buckling (FLB) and Tension Flange Yielding (TFY) limit states in Chapter F of the ANSI/AISC 360 Specification tend to underestimate I-section member flexural resistances as the web and/or the compression flange become increasingly slender. The characterization of FLB only considers the compression flange buckling strength without accounting for its reserve postbuckling capacity. For the TFY limit state, the current equations limit the maximum moment of singly-symmetric slender-web I-section members to the first yield of the tension flange. However, the actual cross-section typically is able to develop extensive yielding of the tension flange and the tension region of the web. The FLB limit state check can be improved by implementing a form of the unified effective width approach, which recognizes the postbuckling resistance of slender flange elements. For the TFY limit state, simple calculations can be configured from mechanics of materials concepts, recognizing the ability of the region in flexural tension to develop extensive spread of yielding. These calculations eliminate the conservatism of the TFY equations while accurately characterizing the associated member structural stability.

This paper proposes updated provisions recognizing the above FLB and TFY limit states behavior, and compares the performance of these provisions to the current limit state equations and to the results from full nonlinear FEA parametric studies. Recommendations are provided for further research to evaluate the impact and implications of these improvements more fully.

1. Introduction
In metal building frames, it is common to use a constant flange width within the fabricated segments of frame members, while stepping the thickness of the flange (as well as tapering of the web depth, and stepping of the web thickness) to achieve significant design economy. In these cases, it is not uncommon for the flanges to be classified as slender by the AISC flexural design rules in the vicinity of inflection points or regions of low bending moment. The current Specification provisions (AISC 2016) do not recognize flange postbuckling strength in flexural compression, although they do account for flange postbuckling strength under uniform axial compression.

---

[1] Graduate Research Assistant, Georgia Institute of Technology, <oguzhantogay@gatech.edu>
[2] Professor, Georgia Institute of Technology, <dwhite@ce.gatech.edu>

The AISC (2016) Compression Flange Local Buckling (FLB) predictions match well with experimental test results for typical cases within the stockier (i.e., smaller $\lambda_f = b_f/2t_f$) range corresponding to inelastic flange local buckling. However, the AISC FLB predictions have been shown to be significantly conservative for flanges classified as slender by the AISC flexural resistance rules. Figure 1 shows comparisons of the AISC predictions to experimental data collected by White and Jung (2008) focusing primarily on inelastic FLB. One can observe from these tests, and from other studies such as Seif and Schafer (2009), that the AISC FLB resistance equations tend to give a conservative estimate of the true FLB resistance for members having a slender compression flange (i.e., $\lambda_f / \lambda_{fr} > 1$). This is due to the substantial postbuckling strength of slender compression flanges. Prior AISC and AASHTO developments have accepted this conservatism. The AASHTO (2017) Specifications limit the flange slenderness to $b_f /2t_f = 12$ as a precaution against flange welding distortion as well as to ensure robustness of rectangular flange plates during fabrication and construction. However, there are applications where a more accurate characterization of slender flange local buckling resistances can be beneficial.
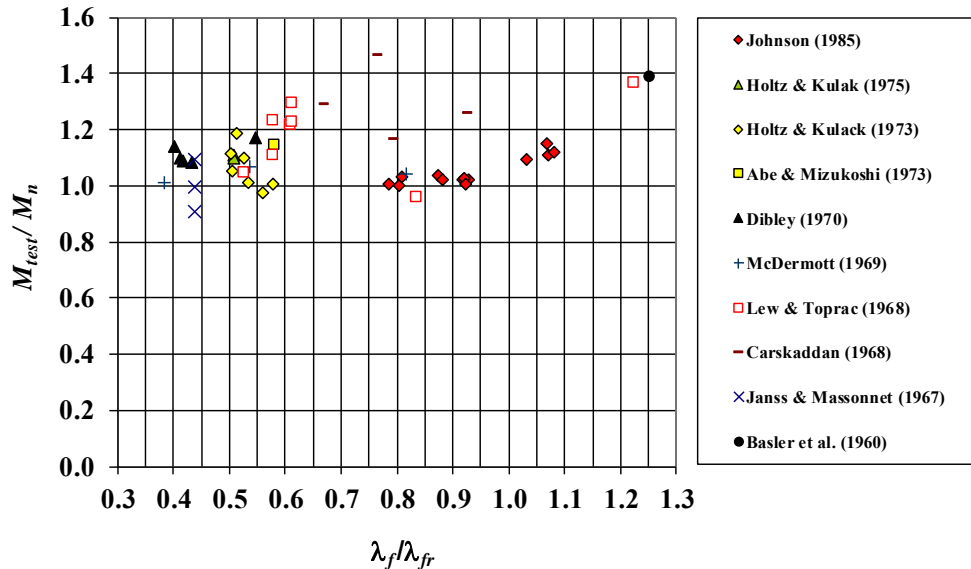
Figure 1: M_{test}/M_n versus λ_f / λ_{fr} for 11 rolled and 36 welded I-section members in which the flexural resistance is governed by FLB, adapted from White and Jung (2008).

Figure 2 compares the AISC (2016) predictions, and recommended predictions discussed subsequently in this paper, to test simulation results from Toğay and White (2017) for a set of identical simply-supported beam-columns with doubly-symmetric cross-sections having a slender compression flange and a noncompact web in flexure (all elements classified as slender in uniform axial compression), subjected to different ratios of primary bending moment and axial compression. The AISC (2016) flexural resistances are governed by the FLB limit state for these members, resulting in up to 30 % conservatism relative to the test simulation results. The test simulation procedures are summarized in the Appendix.

A succinct modification of the current flexural strength provisions to recognize the compression flange postbuckling resistance is possible. An important attribute of the Specification equations that must be preserved is the accurate characterization of FLB resistance, larger than the compression flange yield moment and up to the plastic moment, for I-sections having noncompact flanges and noncompact or compact webs. Approaches in other standards that characterize the FLB postbuckling strength of a slender flange, but then do not recognize the ability of a noncompact

flange section to achieve strengths larger than the yield moment to the compression flange, are deficient for common design situations involving compact or noncompact flanges and webs.
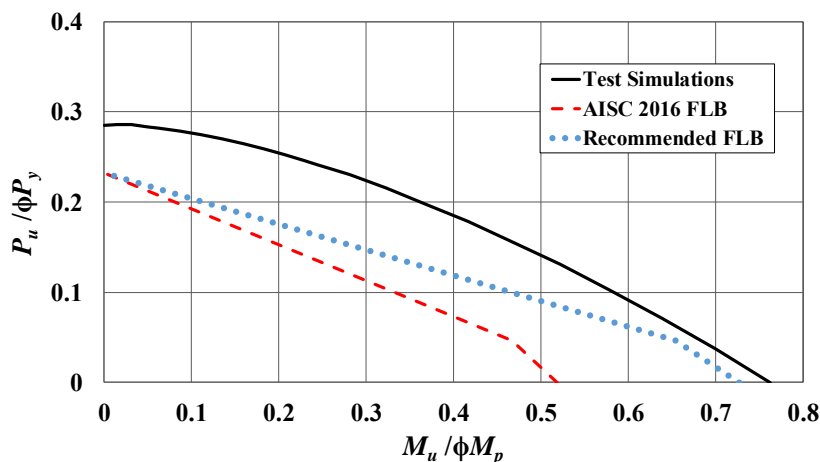
Figure 2: Strength envelopes from test simulation, the AISC (2016) column and FLB flexural strength provisions, and the AISC column and recommended FLB flexural strength provisions, torsionally and flexurally simply-supported doubly-symmetric I-section members with $b_f = 6.5$ in., $t_f = 0.1806$ in. ($b_f/2t_f = 18$), $h = 19.8$ in., $t_w = 0.1787$ ($h/t_w = 111$), and $L_x = L_y = L_z = L_b = 13$ ft, subjected to axial force and moment gradient loading with an applied moment at one end (adapted from Toğay and White (2017)).

For slender-web singly-symmetric members, the AISC Specifications have traditionally employed a Tension Flange Yield (TFY) limit state check simply equal to the yield moment of the tension flange, M_{yt}. In prior practice, metal building engineers have sometimes used singly-symmetric sections with a smaller tension flange to achieve highly optimized designs. These types of sections are physically very efficient, since the depth of web in compression is reduced by shifting of the neutral axis toward the larger compression flange, and since the tension flange does not need to be as large for purposes of design efficiency (because it is in tension rather than in compression). Numerous studies, e.g., Subramanian and White (2017a), have shown that the TFY strength check can be quite conservative for slender-web I-section members. Figure 3 illustrates this conservatism in the AISC (2016) procedures, and improvements gained by the recommended procedures discussed subsequently, relative to test simulation results for a set of simply-supported beam-columns. These 10 ft long members are singly-symmetric and are subjected to uniform primary bending. The right-hand quadrant of the plot corresponds to flexural compression on the larger flange. For this direction of bending, the AISC TFY limit state check governs the flexural resistance for $P_u = 0$. In the left-hand quadrant, the flexural resistance for $P_u = 0$ is governed for these members by FLB. The detailed behavior associated with the strength curves in Fig. 3 is explained in detail for similar members with $L_b = L_x = L_y = L_z = 5$ ft later in the paper.

If a member's web and compression flange are compact, and the member is sufficiently braced, the AISC Specification predicts a flexural capacity equal to the fully plastic moment, M_p. However, in the limit that the web is slender, the Specification has traditionally limited the resistance to the yield moment to the tension flange, M_{yt}. Noncompact-web members are also handled very conservatively in the present Specification as the web becomes thinner.

It is observed that for members where the current TFY limit state controls, eliminating the Tension Flange Yield check and calculating the member yield moment to the compression flange, M_{yc}, accounting for the early spread of yielding within the tension zone, gives a better characterization

3

of the flexural resistance. The modified calculation of M_{yc} can be written in a succinct closed form. This form is the *true* moment at first yielding of the compression flange, and is designated specifically as M_{ycT}, i.e., the yield moment to the compression flange, considering the early yielding of the tension flange and the spread of yielding within the tension zone.
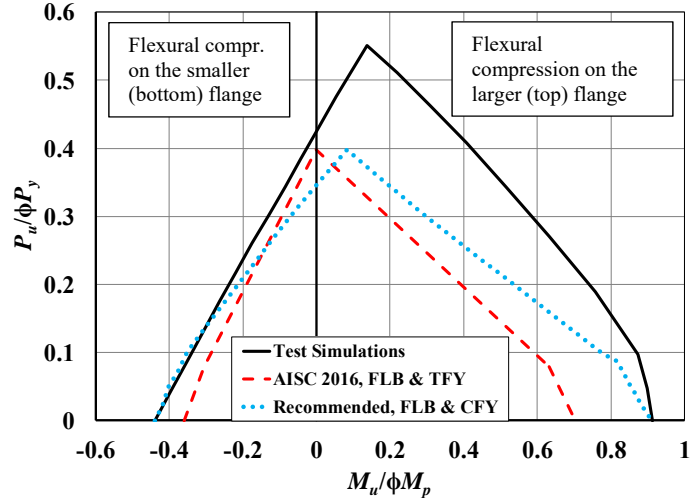
Figure 3: Strength envelopes from test simulation, the AISC (2016) column and flexural strength provisions, and the AISC column and recommended flexural strength provisions, torsionally and flexurally simply-supported singly-symmetric I-section members with $b_{fc} = b_{ft} = 8.0$ in., $t_{fc} = 0.75$ in. $t_{ft} = 0.25$ in., $h = 37.0$ in., $t_w = 0.1875$ in., and $L_x = L_y = L_z = L_b = 10$ ft, subjected to uniform primary bending moment and axial compression.

2. Improved Representation of Flange Local Buckling (FLB) Limit States in Flexure

For cases involving FLB, the conservatism associated with the current buckling-based calculation can be rectified by recognizing the compression flange postbuckling resistance via an application of the unified effective width approach. The following is one way of accomplishing this.

For sections with a slender compression flange in flexure:

a) The effective width of the flange is calculated directly given the flange elastic buckling stress

$$F_{el} = \frac{0.9Ek_c}{(b_f / 2t_f)^2} \tag{1}$$

and the assumption that the compression flange stress within the effective width is F_y at the strength limit in flexure. The terms $F_{e\ell}$ and F_y are substituted into Winter's unified effective width equation,

$$b_e = b_f \left(1 - 0.22\sqrt{\frac{F_{e\ell}}{F_y}}\right)\sqrt{\frac{F_{e\ell}}{F_y}} \tag{2}$$

b) The location of the neutral axis for the effective cross-section, relative to the inside of the compression flange, D_{ce}, and the effective section modulus corresponding to the compression flange, S_{xce}, are determined.

c) The FLB resistance, considering the flange postbuckling strength, is then determined as $R_{pg}M_{yce}$, where M_{yce} is the yield moment to the compression flange for the effective section and R_{pg} is the web bend buckling strength reduction factor, equal to 1.0 for compact- and noncompact-web sections, and calculated as discussed in Section 4 for slender-web sections.

4

For sections having a noncompact flange in flexure:

a) The effective width reduction based on the noncompact flange slenderness limit, λ_{rf}, is applied to the compression flange (regardless of the actual flange slenderness), and the corresponding $R_{pg}M_{yce}$ is determined using the procedure explained above. This establishes an "anchor point" corresponding to the flange postbuckling resistance at $\lambda = \lambda_{rf}$, labeled as $M_{yce(\lambda r)}$ in Fig. 4.

b) A modified linear interpolation is then employed between the anchor points (λ_{rf}, $M_{yce(\lambda r)}$) and (λ_{pf}, M_{maxFLB}), where M_{maxFLB} is the plateau resistance equal to M_p for a compact-web section, $R_{pc}M_{yc}$ for a noncompact-web section, and $R_{pg}M_{yc}$ for a slender web section. This gives the improved estimate of the inelastic FLB resistance illustrated in Fig. 4. (Note: M_{ycT} is substituted for M_{yc} in the case of cross-sections that exhibit early tension flange yielding.)
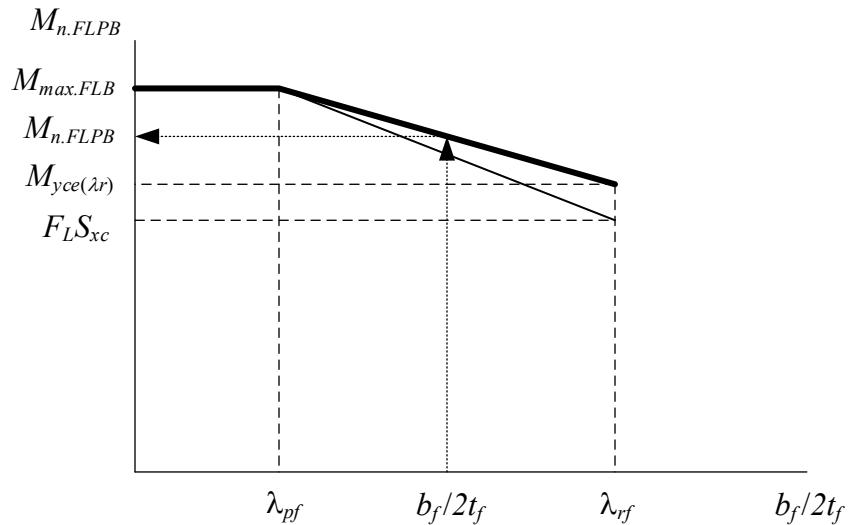
Figure 4: Calculation of compression flange local postbuckling (FLPB) resistance within the inelastic FLB range.

The above calculation preserves the clear qualities of the AISC FLB resistance calculations in for common cases with noncompact and compact I-section flanges, while recognizing the additional resistance associated with the flange local postbuckling response of slender flanges. White and Jung (2008) and White and Kim (2008) report reliability indices for FLB that are somewhat larger than the target value of 2.6 for statically determinate beam tests, based on the current AISC (2016) FLB equations. The above update results gives a reliability index estimates closer to 2.6.

The updates mentioned above significantly improve the FLB resistance predictions corresponding to $P_u = 0$ in Figs. 2 and 3. The updates also improve the overall prediction of the strengths under combined flexure and axial load. It should be noted that the strength predictions for high axial load cannot be improved significantly relative to the results shown here unless a more accurate column strength curve were adopted. An improved representation of the shape of the beam-column strength curve can be obtained by using Inelastic Buckling Analysis (White et al. 2016).

3. Improved Consideration of Tension Flange Yielding (TFY)
When a singly-symmetric section is subjected to flexure with the larger flange in compression, the flexural resistance can be governed by tension flange yielding (TFY). If the section has a slender-web, the TFY resistance can be quite conservative. While the AISC (2016) TFY limit is equal to the plastic moment capacity ($\phi_b M_p$) for compact-web I sections, the TFY limit is equal to the tension flange yield strength ($\phi_b M_{yt}$) for slender-web sections.

For cases in which first yielding is encountered at the tension flange (and for which the TFY resistance check is currently employed), one can account for the early yielding on the tension side of the neutral axis in the calculation of the yield moment to the compression flange. This modified yield moment is referred to as M_{ycT}. A representative flexural stress profile associated with this calculation is shown in Figure 5. Mechanistically, the use of M_{ycT} is more rigorous than the use of M_{yc}, since M_{ycT} captures the influence of yielding on the tension side of the neutral axis. This modified yield moment can be employed with the FLB calculations discussed previously, as well as within the LTB equations, to provide an accurate characterization of the FLB and LTB limit states, including the impact from early yielding in flexural tension. The TFY limit state calculations are in effect folded into the determination of M_{ycT}. No explicit TFY limit state check is required in this updated approach. The resulting calculations are explained further below.

A simple set of equations can be derived for the calculation of M_{ycT} by working with the flange forces at the flange centroids, rather than considering rectangular stress blocks associated with the flange forces (see Fig. 5). This streamlined calculation of M_{ycT} requires the distance between the neutral axis and the center of the compression flange, a. This variable is determined such that the net longitudinal force from the stress distribution in Fig. 5 is equal to zero:

$$a = \frac{\Delta A + \sqrt{(\Delta A)^2 - t_{fc}^2 t_w^2}}{4 t_w} \tag{3a}$$

where:

$$\Delta A = t_w h + b_{ft} t_{ft} + t_{fc} t_w - b_{fc} t_{fc} \tag{4}$$

Given a, the depth of the web in compression, D_{cT}, is obtained as shown in Fig. 5.
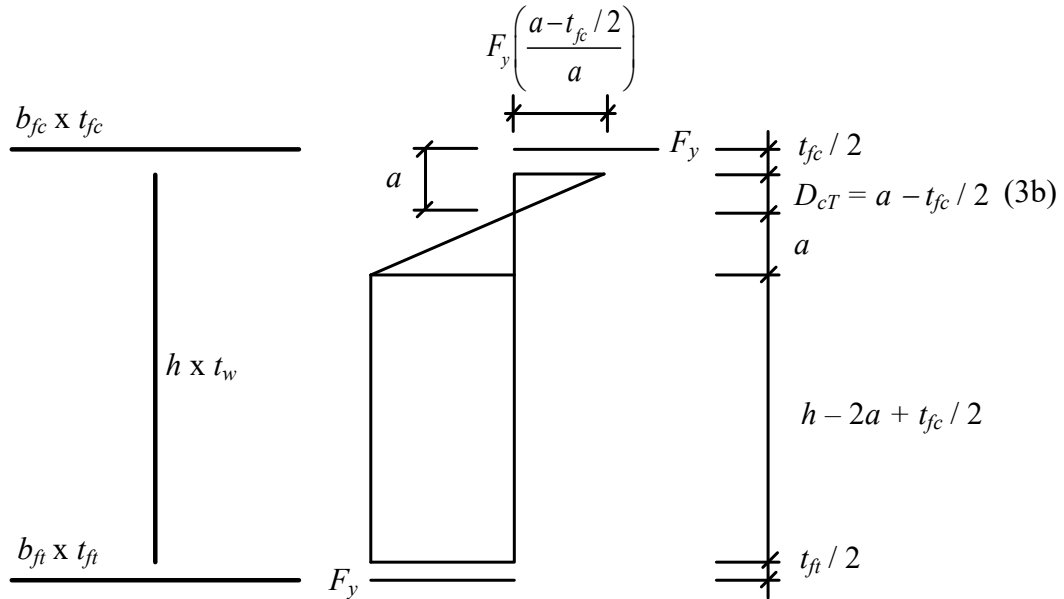
Figure 5: Representative flexural stress profile associated with the calculation of M_{ycT}, considering early yielding on the tension side of the neutral axis.

Interestingly, the depth of the web in compression for the fully-plastic cross-section, D_{cp}, can be used as an estimate for D_{cT} with a maximum error of approximately 1 % for all practical I-section dimensions. Therefore, it is recommended that D_{cT} be taken as

$$D_{cp} = \frac{t_w h + b_{ft} t_{ft} - b_{fc} t_{fc}}{2t_w} \qquad (5)$$

Using $D_{cT} \approx D_{cp}$, M_{ycT} is obtained as

$$M_{ycT} = F_y \begin{bmatrix} b_{fc} t_{fc} a + \dfrac{D_{cT}^{\,3}}{3a} t_w + \dfrac{a^2}{3} t_w + \dfrac{(h - a - D_{cT})^2}{2} t_w \\ + (h - a - D_{cT}) t_w a + b_{ft} t_{ft} (h_o - a) \end{bmatrix} \qquad (6)$$

by summing the moment contributions from the stress blocks in Fig. 5. The $D_{cT} \approx D_{cp}$ approximation is valid for $D_{cp} \geq 0$. For cases where D_{cp} in Eq. 5 becomes negative, the plastic neutral axis is located in the compression flange and the neutral axis associated with first yielding of the compression flange also tends to be in the compression flange. For this case, M_{ycT} may be approximated with good accuracy as the fully plastic moment M_p.

Given the above calculations of D_{cT} and M_{ycT}, these values are substituted for the terms D_c and M_{yc} in the flowcharts presented in Section 4, which detail the recommended unified calculation of the flexural resistance for general homogeneous I-section members.

4. Recommended Changes to the Unified Flexural Resistance Provisions

White (2008) provides a detailed overview of the so-called "unified flexural resistance provisions" developed as part of the major updates to the AASHTO LRFD Specifications in 2004 and the AISC Specification in 2005. White (2008) provides flowcharts that illustrate the overall organization of the unified calculations. Minor differences between the finalized AASHTO and AISC provisions and the unified provisions are explained where they occur.

Figures 6 through 8 show a modified form of the flowcharts from White (2008). These updated flowcharts implement the recommended changes discussed above in Sections 2 and 3 in the context of homogeneous I-section members. Hybrid I-section members are addressed further in Toğay (2018). Furthermore, these flowcharts implement updates to the AISC LTB resistance calculations recommended by Subramanian et al. (2018) necessary to address low reliability index estimates in the intermediate inelastic LTB range, particularly for welded I-section members. The flowcharts in Figs. 6 through 8 utilize the terms D_c and M_{yc} for the depth of the web from the inside of the compression flange to the neutral axis at the nominal first yielding of the compression flange and the yield moment to the compression flange, respectively. The corresponding values D_{cT} and M_{ycT} discussed in Section 3 are substituted into D_c and M_{yc} in cases where early yielding occurs at the tension flange, i.e., when $M_{yt} < M_{yc}$. (It should be noted that S_{xc} in Figs. 6 to 8 is the elastic section modulus to the compression flange, without any consideration of early tension flange yielding.) All the variables in Figs. 6 to 8 are expressed using the AISC (2016) notation, with the exception of $2D_c$, which is expressed in the AISC Specification as h_c. The term R_{pg} is denoted by R_b and the term F_L (the "nominal compressive strength above which the inelastic buckling limit states apply") is denoted by F_{yr}, in AASHTO (2017).

The recommended modifications to the original "unified" flowcharts are as follows:
- In Eq. 8 (see Fig. 6), the coefficient 5.7 in the corresponding AISC (2016) equation is replaced by the coefficient c_{rw}. This coefficient is defined in Eq. 9. This modification is based on observations by Subramanian and White (2017b), from physical tests and test simulations, that

I-girders with relatively small flanges compared to the web area exhibit a minor reduction in their flexural resistances when their webs are near the current noncompact web limit. That is, noncompact-web girders of this nature tend to perform more like slender-web girders.

- In the flowchart cells containing Eqs. 13 and 14, and 22 through 25, the calculation of R_{pt} is eliminated. The recommended calculations no longer require any explicit calculation of Tension Flange Yielding (TFY). The TFY response is folded into the calculation of $M_{yc} = M_{ycT}$ for cross-sections having a larger compression flange such that $M_{yt} < M_{yc}$.

$$c_{rw} = \max\left[\min\left(4.6,\ 3.1 + 2.5\frac{b_{fc}t_{fc}}{D_c t_w} \right), 5.7 \right] \quad (9)$$

$$F_{yf} \le 70 \text{ ksi} \quad (7)$$

$$\frac{2D_c}{t_w} \le \left[\lambda_{rw} = c_{rw}\sqrt{\frac{E}{F_{yc}}} \right] \quad (8) \quad \&$$

$$\frac{I_{yc}}{I_{yt}} \ge 0.3 \quad (10)$$

Eq. (10) applies only to noncomposite sections

No (slender web)

$$R_{pg} = \min\left[1,\ 1 - \frac{a_{wc}}{1200 + 300a_{wc}}\left(\frac{2D_c}{t_w} - \lambda_{rw} \right) \right] \quad (16)$$

$$a_{wc} = \frac{2D_c t_w}{b_{fc}t_{fc}} \quad (17) \qquad R_{pc} = 1 \quad (18) \qquad ①$$

$$F_L = 0.5F_{yc} \quad (19) \quad \text{for LTB}$$

Go to A

Yes (compact or noncompact-web)

$$m = \frac{1}{\left(0.54\dfrac{M_p}{M_{yc}} - 0.09 \right)^2} \quad (12)$$

$$\frac{2D_{cp}}{t_w} \le \left[\lambda_{pw} = \min\left(m\sqrt{\frac{E}{F_{yc}}},\ \lambda_{rw}\frac{D_{cp}}{D_c} \right) \right] \quad (11)$$

No (noncompact web)

$$\lambda_{pw(D_c)} = \min\left(\lambda_{pw}\frac{D_c}{D_{cp}},\ \lambda_{rw} \right) \quad (20) \qquad \lambda_w = \frac{2D_c}{t_w} \quad (21)$$

$$R_{pc} = \left[1 - \left(1 - \frac{M_{yc}}{M_p} \right)\left(\frac{\lambda_w - \lambda_{pw(D_c)}}{\lambda_{rw} - \lambda_{pw(D_c)}} \right) \right]\frac{M_p}{M_{yc}} \le \frac{M_p}{M_{yc}} \quad (22)$$

$$R_{pg} = 1 \quad (23)$$

Yes (compact web)

$$R_{pc} = \frac{M_p}{M_{yc}} \quad (13)$$

$$R_{pg} = 1 \quad (14)$$

$$F_L = 0.5F_{yc} \quad (15) \quad \text{for LTB}$$

Go to A

① $R_{pg} = 1$ is permitted for longitudinally-stiffened girders in which web bend buckling is prevented at a compression flange stress of F_{yc}

Figure 6: Calculation of the web slenderness based parameters, R_{pc} and R_{pg}, and the nominal compressive strength above which inelastic buckling limit states apply, F_L.

- Equations 15 and 19 are modified to $F_L = 0.5F_{yc}$ pertaining to Lateral Torsional Buckling. This is based on the recommendations from Subramanian et al. (2018) addressing low reliability index estimates in the intermediate inelastic LTB range. Engineers often consider F_L to simply represent residual stress effects. However, there is far more to F_L than just the consideration of residual stresses. This term also accounts for the reduction in the LTB capacity at intermediate unbraced lengths due to amplification of initial geometric imperfections by stability effects. It should be noted that the updated provisions no longer require F_L in the determination of the FLB resistance, other than in the calculation of λ_{rf} where it is recommended that F_L for FLB may be taken simply as $0.7F_y$ for homogeneous cross-section members. The term $F_L S_{xc}$ is replaced by $M_{yce(\lambda r)}$ as discussed below
- The noncompact web slenderness limit is employed in the last term of Eq. 17 for R_{pg}. This is consistent with the form of the unified equations implemented in AISC (2016), but using the variable coefficient c_{rw} in the expression for λ_{rw}.
- Equation 30 in Fig. 7 is modified by replacing the original term $F_L S_{xc}$ by $M_{yce(\lambda r)}$. This implements the enhancement illustrated previously in Fig. 4.
- Equation 31 in Fig. 7 is modified from the theoretical elastic FLB equation to the yield moment to the compression flange in the effective cross-section, accounting for residual stress and geometric imperfection effects via Winter's plate effective width equation, Eq. 2.
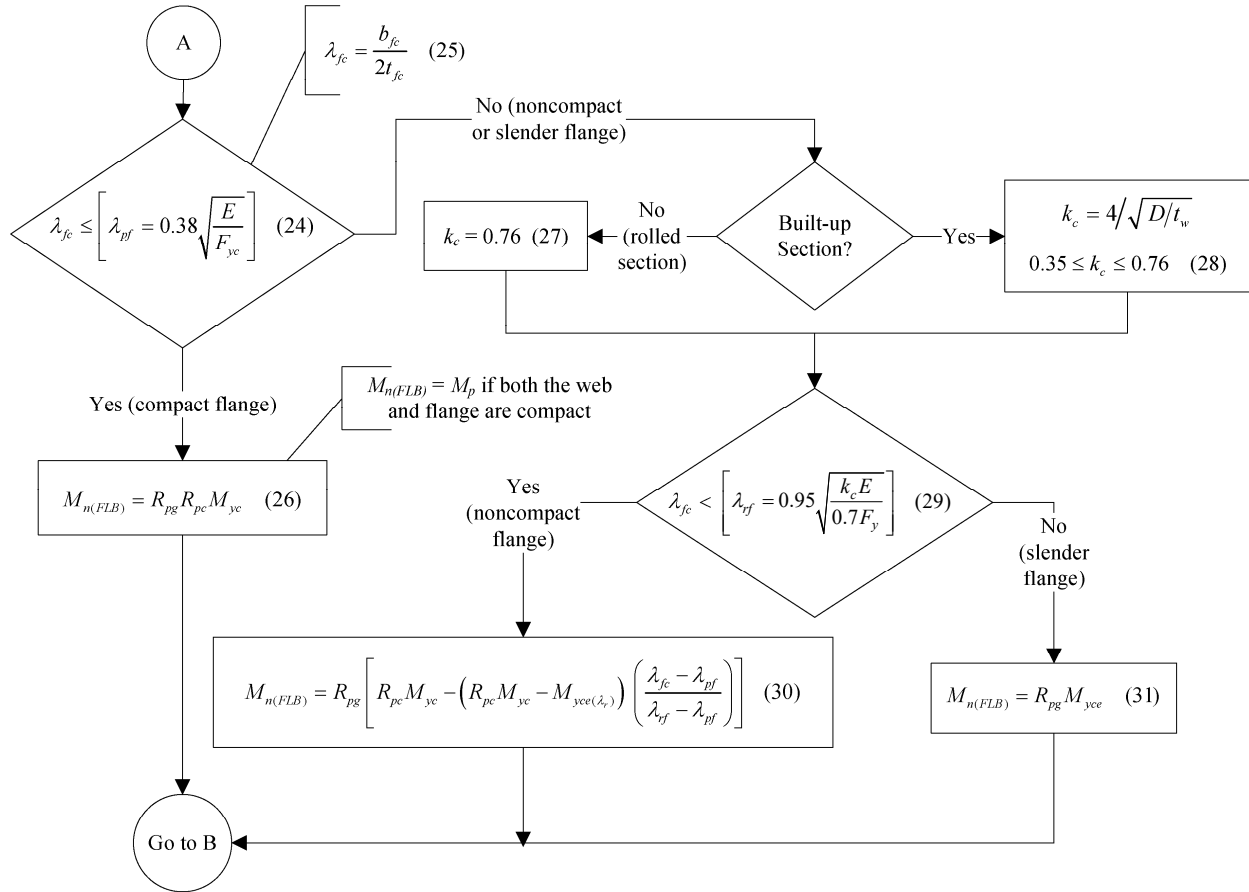
Figure 7: Flange Local Buckling strength calculations.

- Equation 32 in Fig. 8 is modified from the original unified equation for L_p to again address low reliability index estimates in the intermediate inelastic LTB range (Subramanian et al. 2018). In addition, this modified equation recognizes that test simulations commonly show a smaller "plateau length" than indicated by the original unified provisions (Subramanian and White 2017c, 2017d; Kim 2010; Greiner and Kaim 2001).
- Equations 38 and 41 specify the limit on the moment above which inelastic buckling limit states apply. This moment is taken as $F_L S_{xc}$ as in the prior unified provisions. However, in the case of highly singly-symmetric cross-sections with the larger flange in compression, $M_{yc} = M_{ycT}$ potentially can be smaller than $F_L S_{xc}$. In this extreme case, M_{ycr} is taken equal to M_{ycT}.
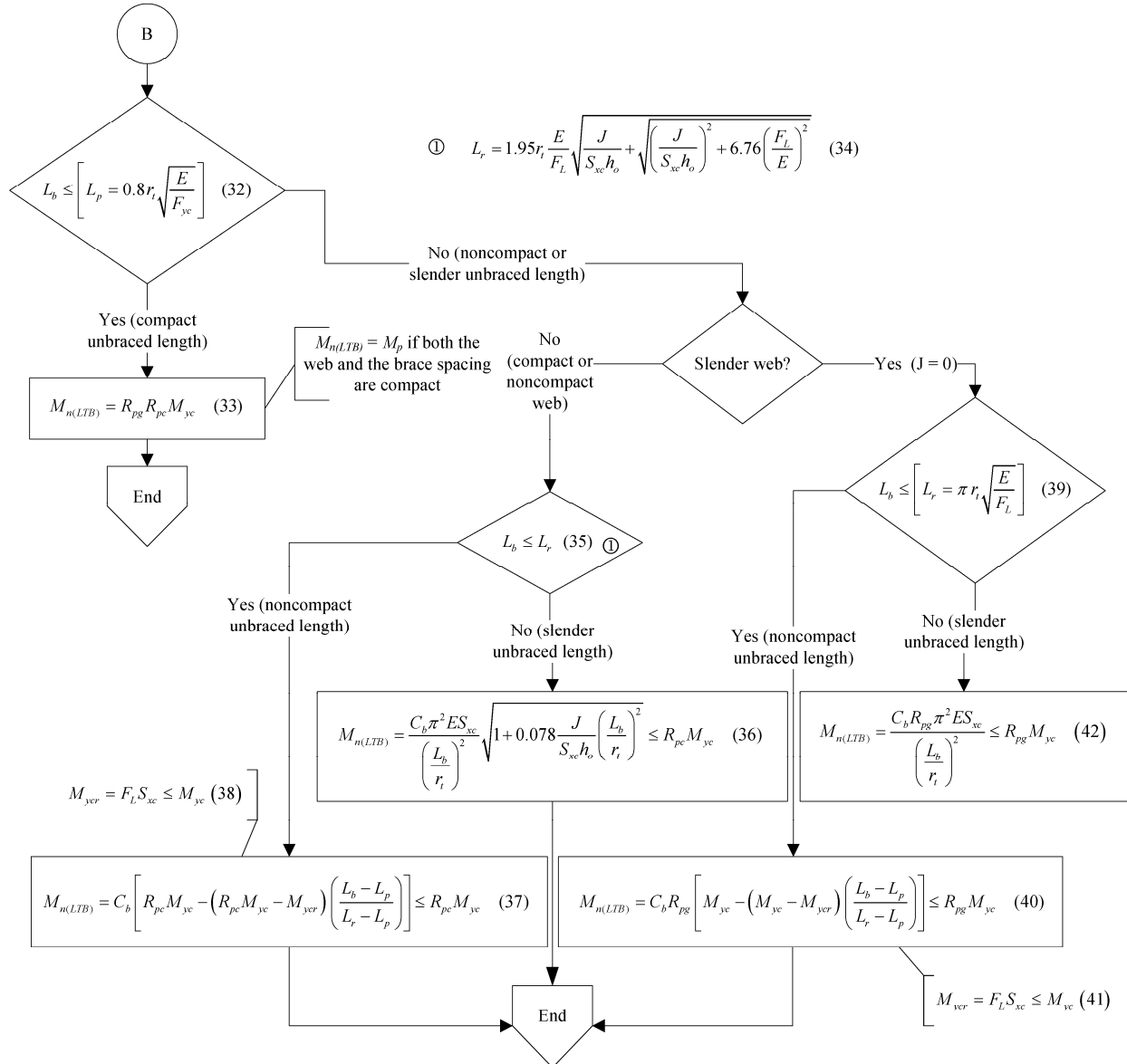
Figure 8: Lateral Torsional Buckling strength calculations

White (2008) shows a fourth flowchart for the calculation of $M_{n(TFY)}$. As stated above, the TFY limit state check is replaced by the consideration of early yielding in flexural tension in the calculation of the yield moment to the compression flange, M_{ycT}. This relegates Tension Flange

Yielding to a secondary role in the calculation of the flexural resistance, similar to the manner that the original unified flexural resistance equations relegated Web Local Buckling to a secondary role in the calculation of the FLB and LTB resistances.

5. Beam-Column Strength Interaction
With one change regarding exceptional cases, it is recommended to address the interaction of axial and flexural resistance using the AISC (2016) bilinear strength interaction equations H1-1a and H1-1b, as illustrated in Figs. 2 and 3. The exceptional cases and the recommended change for these cases are discussed below in Section 6. The true beam-column strength envelopes for general singly-symmetric I-sections can be rather complex. However, deficiencies in the strength predictions for high axial compression are often driven in part by the use of a single column strength curve to represent the axial compressive resistance. Without improving the accuracy of the column strength estimates, improvements in the accuracy of beam-column resistances are often limited.

As noted previously, improvements in the representation of the shape of beam-column strength curves can be obtained by using Inelastic Buckling Analysis (White et al. 2016). However, this paper focuses on manual calculations and their comparison to test simulation results.

6. Comprehensive Example Illustrating Recommended Compression Flange Buckling and Tension Flange Yielding Improvements
A detailed example is presented in this section to demonstrate the calculations outlined in Sections 2 and 3, and to compare the resulting predictions to the limit states response determined by test simulation. This example is the same as in Fig. 3, except $L_b = L_x = L_y = L_z = 5$ ft here. The particular cross-section studied is from a clear-span metal building frame design shared with the authors. Similar to Fig. 3, Fig. 9 compares the current AISC (2016) and the recommended strength predictions to the results from test simulation.
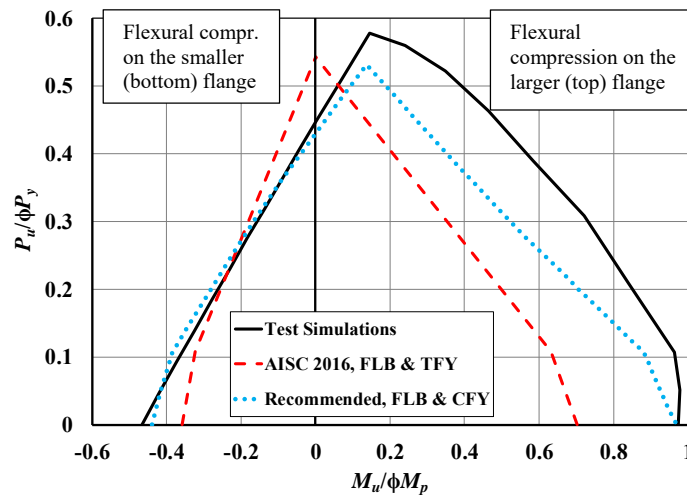
Figure 9: Strength envelopes from test simulation, the AISC (2016) column and flexural strength provisions, and the AISC column and recommended flexural strength provisions, torsionally and flexurally simply-supported singly-symmetric I-section members with $b_{fc} = b_{ft} = 8.0$ in., $t_{fc} = 0.75$ in. $t_{ft} = 0.25$ in., $h = 37.0$ in., $t_w = 0.1875$ in., and $L_x = L_y = L_z = L_b = 5$ ft, subjected to uniform primary bending moment and axial compression.

With the current AISC (2016) Specification, the flexural resistance for $P_u = 0$ is limited by TFY for flexure causing compression on the larger flange (i.e., for the curve in the right-hand quadrant of the plot). It is limited by FLB for flexure causing compression on the smaller flange (corresponding to the left-hand quadrant of the plot). However, with the recommended provisions, the

flexural resistance in the right-hand quadrant is limited by LTB while the flexural resistance in the left-hand quadrant is limited by Flange Local Postbuckling (FLPB). The AISC (2016) TFY check is 28% conservative relative to the corresponding test simulation strength in the right-hand quadrant for $P_u = 0$ while the AISC (2016) FLB check is 23% conservative relative to the test simulation results in the left-hand quadrant. The recommended calculations are 0.5% and 6% conservative relative to the test simulation results for $P_u = 0$.

6.1 Results from intermediate and final resistance calculations
The results of the various intermediate and final resistance calculations are listed below:

- *Cross-section dimensions & width-to-thickness ratios*

Top flange: $b_f = 8$ in., $t_f = 0.75$ in., $b_f/2t_f = 5.33$
Bottom flange: $b_f = 8$ in., $t_f = 0.25$ in., $b_f/2t_f = 16.0$
Web: $h = 37$ in., $t_w = 0.1875$ in., $h/t_w = 197$

For bending causing compression on the larger flange: $D_c = 13.4$ in., $2D_c/t_w = 143$, $D_{cp} = 7.83$ in. (Eq. 5), $D_{cT} = 0.999D_{cp}$ (Eq. 3b in Fig. 5), $2D_{cT}/t_w = 83.5$

For bending causing compression on the smaller bottom flange: $2D_c/t_w = 252$

- *Overall cross-section properties*

$F_y = 55$ ksi, $I_x = 3236$ in^4, $S_{xc} = 229$ in^3, $S_{xt} = 136$ in^3, $M_{y.top} = 1047$ ft-kip, $M_{y.bot} = 622$ ft-kip, $M_p = 886$ ft-kip, $M_p/M_{y.top} = 0.846$, $M_p/M_{y.bot} = 1.42$

For bending causing compression on the larger top flange: $M_{ycT} = 870$ ft-kip

Note that the yield moment to the top flange, $M_{y.top}$, is actually larger than the fully-plastic moment for this section. This is due to the neglect of the early onset of yielding at the bottom flange in this traditional calculation per AISC and AASHTO. The AISC and AASHTO resistance equations in whole account for the early yielding at the bottom flange in this type of section, but they tend to handle this attribute of the strength behavior conservatively via a relatively elaborate implementation of the R_{pc} and R_{pt} factors.

- *Flange slenderness limits (Table B4.1 of the AISC (2016) Specification)*

$\lambda_{pf} = 8.73$ and $\lambda_{rf} = 15.4$ (flexure), $\lambda_{rf} = 8.69$ (axial compression)

The larger top flange of the subject cross-section is nonslender under uniform axial compression and compact under flexure. This means that local buckling of this flange is not a factor in the calculation of the resistances for any combination of axial load and moment.

The smaller inside flange is slender under both uniform axial compression and flexure. This indicates that local buckling of this flange is a significant factor in the resistance under both uniform axial compression and flexure causing compression on the inside flange.

The recommended provisions are the same as the AISC (2016) provisions with regard to the above limits, with the exception that the term F_L is expressed simply as $0.7F_y$ in the recommended provisions. This is made possible by the consideration of TFY directly in the calculation of M_{ycT}.

- *Web slenderness limits*

AISC (2016) nonslender web limit for uniform axial compression: $\lambda_{rw} = 34.2$ (Table B4.1a)

This limit is the same for the recommended and the AISC (2016) calculations. The web is classified as slender under uniform axial compression.

AISC (2016) noncompact web slenderness limit in flexure: $\lambda_{rw} = 5.7\sqrt{E/F_y} = 131$ (Table B4.1b)

Recommended noncompact web slenderness limit in flexure (Subramanian and White 2017b):
When the larger top flange is in flexural compression: $A_{fc} = 6$ in^2, $A_{wc} = 2.51$ in^2, $A_{fc}/A_{wc} = 2.39$, $c_{rw} = 5.7$ (Eq. 9), $\lambda_{rw} = 131$ (Eq. 8)

When the smaller bottom flange is in flexural compression: $A_{fc} = 2$ in^2, $A_{wc} = 4.42$ in^2, $A_{fc}/A_{wc} = 0.452$, $c_{rw} = 4.6$ (Eq. 9), $\lambda_{rw} = 106$ (Eq. 8)

AISC (2016) compact web slenderness limit in flexure:
When the larger top flange is in flexural compression: $\lambda_{pw} = 85.2$ (Table B4.1b)

When the smaller bottom flange is in flexural compression: $\lambda_{pw} = 40.3$ (Table B4.1b)

Recommended compact web slenderness limit in flexure:
When the larger top flange is in flexural compression: $m = 4.69$ (Eq. 12), $\lambda_{pw} = 108$ (Eq. 11)

When the smaller bottom flange is in flexural compression: $m = 2.17$ (Eq. 12), $\lambda_{pw} = 49.8$ (Eq. 11)

AISC (2016) web classification in flexure:
When the larger top flange is in flexural compression, since $(2D_c/t_w = 143) > (\lambda_{rw} = 131)$ the web of the subject cross-section is slender in flexure.

When the smaller bottom flange is in flexural compression, since $(2D_c/t_w = 252) > (\lambda_{rw} = 131)$ the web of the subject cross-section is slender in flexure.

Recommended web classification in flexure:
When the larger top flange is in flexural compression, since $(2D_{cT}/t_w = 83.5) < (\lambda_{pw} = 108)$, the web is compact in flexure.

When the smaller bottom flange is in flexural compression, since $(2D_c/t_w = 143) > (\lambda_{rw} = 106)$, the web is slender in flexure.

- *Governing FLB and FLPB flexural resistances for compression on the smaller bottom flange*
AISC (2016) calculations: $R_{pg} = 0.789$ (Eq. F5-6), $a_w = 4.42$ (Eq. F4-12), $F_{cr} = 35.7$ ksi (Eq. F5-9), $\phi M_{n(FLB)} = 287$ ft-kip (Eq. F5-7), and $\phi M_{n(FLB)} / \phi M_p = 0.359$

Recommended calculations: $R_{pg} = 0.744$ (Eq. 16), $a_w = 4.42$ (Eq. 17), $b_{fe} = 5.30$ in. (compression flange) (Eq. 2), $S_{xce} = 114$ in.^{3}, $\phi M_{n(FLB)} = 349$ ft-kip (Eq. 31), and $\phi M_{n(FLB)} / \phi M_p = 0.438$

- *Governing TFY and LTB flexural resistances for compression on the larger top flange*
AISC (2016) calculations: $\phi M_{n(TFY)} = 560.05$ ft-kip (Eq. F5-10)

Recommended calculations: $M_{ycT} = 867$ ft-kip (Eq. 6), $m = 4.69$ (Eq. 12), $R_{pc} = 1.02$, $\phi M_{n(LTB)} = 782$ ft-kip (Eq. 37), $\phi M_{n(LTB)} / \phi M_p = 0.975$

- *Member axial compressive resistance*:
AISC (2016) calculations: $F_e = 227$ ksi (Eq. E3-4), $F_{cr} = 49.7$ ksi (Eq. E3-2), $b_e = 8.46$ in. for the web (Eq. E7-3), $b_e = b = 8.00$ in. for the larger top flange (Eq. E7-2), $b_e = 5.54$ in. for the smaller bottom flange (Eq. E7-3), $A_e = 8.97$ in.^{2}, $\phi P_n = 401$ kips (Eq. E7-1), $\phi P_n / \phi P_y = 0.54$

6.2 Discussion of Overall Results

The following are key observations that can be highlighted regarding the final strength curves shown in Fig. 9:

- Members having the above dimensions are able to develop very close to the factored plastic moment resistance of the cross-section at low axial force levels, when the larger compact (top) flange is in flexural compression. This is evidenced by the intersection of the solid curve with the horizontal axis on the right-hand side of the plot. The recommended modification of the AISC (2016) provisions predicts the test simulation strength in flexure alone quite well. The current AISC provisions are quite conservative for this loading case. This is due to the fact that the current provisions limit the flexural resistance of this cross-section to the nominal first yielding of the tension flange, $\phi_b M_{yt}$.
- Figure 10 shows the contours of the plastic equivalent strain (PEEQ) at the mid-surface of the component plates at the peak load, for the case of $P_u = 0$ and flexural compression on the larger top flange. The darkest contour indicates the locations that are still elastic at this stage. The other contours indicate different magnitudes of yielding. It can be observed that at this load level, the bottom flange, the majority of the top flange, and more than half of the web have yielded. In Fig. 5, the recommended design model predicts the onset of yielding at a depth of $2a = 2D_{cT} + t_{fc} = 16.4$ in. below the centroid of the top flange at the first yield to the compression flange for this section. This is 43% of the total depth between the flange centroids. This value matches well with the extent of the elastic region shown in Fig. 10. The internal moment from the test simulation at the peak load is only slightly less than ϕM_p, and it is in fact approximately equal to ϕM_{ycT}, which is itself only slightly less than ϕM_p.
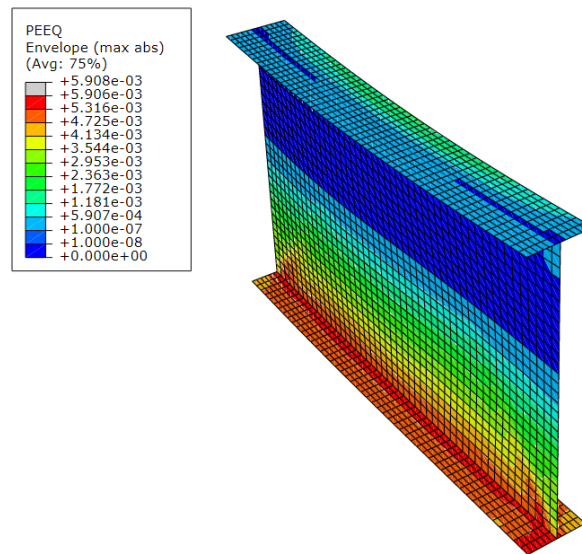
Figure 10: PEEQ (plastic equivalent strain) contours on the deflected shape for example singly-symmetric I-section member subjected to uniform moment loading causing compression on the top flange ($P_u = 0$).

- The flexural resistance for the above $P_u = 0$ case is predicted quite accurately considering the reductions for the noncompact web and for inelastic LTB, and the reductions due to extensive yielding in the tension zone captured by the yield moment to the compression flange, M_{ycT}. It should be noted that if the AISC (2016) LTB equations are employed without the modifications in Eqs. 9, 15, 19 and 32, they generally tend to over-estimate the test simulation results (Subramanian and White, 2017a, 2017b, 2017c, 2017d; 2017e; Subramanian et al., 2018).
- For flexure causing compression on the larger compact (top) flange in the above members, there is a minor increase in the physical flexural resistance with the addition of a small amount of axial compression,. This is due to a reduction in yielding on the side of the neutral axis in

14

flexural tension, due to the added axial compression. However, the cross-section is already yielded extensively at these strength limits. Therefore, the enhancement in strength is very minor compared to what one would expect by considering theoretical elastic stresses and strength of materials equations. The AISC Eqs. H1-1a and H1-1b are far from perfect in capturing this behavior. However, with the recommended enhancements in the flexural resistance calculations, the corresponding beam-column resistances are substantially larger than with the current provisions. Given that $P_u/\phi P_y$ is typically less than about 0.2 in metal building frames, the recommended enhancements are quite effective at capturing the true capacities in the context of metal building frame members.

- Considering the case of flexural compression on the smaller slender (bottom) flange with zero axial compression, the test simulations show 37 % larger strength than obtained using the AISC (2016) FLB equations (or as noted above, the AISC (2016) FLB check is 23% conservative relative to the test simulation results). This is due to the lack of recognition of compression flange local postbuckling strength in the current provisions. The recommended provisions recognize this additional source of resistance, and predict the test simulation results with only minor conservatism. It should be noted that flexural compression on the smaller (bottom) flange is not a likely loading scenario for the cross-section considered in this example. However, the results are representative of those for more practical cross-sections, say in the vicinity of an inflection point in a frame, where both flanges may be relatively thin.

- The rigorous beam-column strength interaction shown by the solid curve on the left-hand side of the plot, obtained from the test simulation studies, is essentially linear for all practical purposes. Both the recommended and the current application of AISC Eqs. H1-1a and H1-1b extend slightly above this rigorous curve (i.e., they are slightly unconservative) at two different locations. The dotted (recommended) curve extends slightly above the rigorous curve within the vicinity of the "knee" of Eqs. H1-1. This is due to the fact that the true interaction is closer to linear. However, the conservatism of the AISC column strength curve (i.e., $\phi_c P_n$) for these members results in the predictions using Eqs. H1-1 still being reasonably good using the recommended calculations. Conversely, the current AISC (2016) prediction (i.e., the dashed curve) extends somewhat more markedly above the rigorous solid curve at high axial load levels. This is due to the fact that, under high axial compression, the small slender (bottom) flange and the web adjacent to this flange have a significant reduction in their effective areas. This effective area reduction, which occurs just on the bottom side of the members, results in a shift of the effective centroid and an introduction of an effective eccentricity of the axial compression force relative to this effective centroid. For the recommended (dotted) interaction curve, the combination of the conservative $\phi_c P_n$ and the inclusion of this effective eccentric moment from the axial compression results in an accurate prediction, avoiding the unconservatism in the predictions from the current AISC (2016) provisions.

- It should be noted that the moment, M_u, on the horizontal axis of the plot does not include the above additional internal moment, due to the eccentricity of the applied axial loads with respect to the effective centroidal axis of the cross-section under high axial compression. The additional internal eccentric moment causes a shift in the strength curve. One can observe that the peak $P_u/\phi P_y$ point on both the dashed AISC (2016) curve and the dotted recommended curve are at the same value, i.e., approximately 0.54. This corresponds to the AISC (2016) axial compressive resistance of these members, governed by flexural-torsional buckling. The test simulations predict a somewhat larger axial compressive resistance of these members.

- The behavior of these members, if we consider the cases starting with $M_u = 0$ (where the strength curves cross the vertical axis) and as we start to apply small $M_u > 0$, causing flexural compression on the larger compact (top) flange, is that the resulting net compressive stresses on the smaller slender (bottom) flange are reduced. This results in an overall net increase in the axial compressive resistance due to the application of small $M_u > 0$ to the members. However, once we have applied a little less than $M_u = 0.2\phi M_p$ to the members, the increasing compression on the top flange becomes more dominant in its effect on the member ultimate strength. Hence, for M_u larger than about $0.2\phi M_P$, the subject members start to support less and less P_u with increasing M_u.
- It appears that the maximum $P_u/\phi P_y$ point, on the dotted (recommended) design strength curve and on the solid (rigorous) test simulation based strength curve, occur at roughly the value of M_u that is equal and opposite to the eccentric moment caused by the axial force acting through the eccentricity between its line of action and the effective centroid of the cross-section (where we have lost significant effective area on the side of the cross-section corresponding to the smaller (slender) bottom flange.
- It should be noted that the AISC (2016) *Specification* and commentary do not address the impact of the axial load eccentricity due to loss of effective area on singly-symmetric cross-section members. The AISI (2012) Specification did speak to this issue, although the AISI (2016) Specification is now silent about it. The original development of the unified effective width method (Peköz (1986)) showed that accurate predictions were obtained for general singly-symmetric and unsymmetric beam-columns, with the exception of slender angle sections, when the moment of the axial loads is taken about the centroidal axis of the effective section determined considering axial load alone. AISI (2016) relaxes the requirement that the bending moment should be defined with respect to the centroidal axis of the effective section. The increased eccentricity due to local buckling can have a measurable impact on the resistance of in an ideally pin-ended member; however, this effect tends to become minor in continuous members or members with ends restrained, where the rotations due to these eccentricities are restrained. As stated above, AISC (2016) also neglects these effects. An additional eccentric bending moment may be included in Eqs. H1-1, to account conservatively for potential situations where shifting of the cross-section effective centroidal axis due to local buckling may have a measurable impact on compression member resistances. This practice parallels the handling of these effects in CEN (2006). It is included here to obtain the best correlation with the test simulation results, where the ends of the unbraced lengths are assumed to be flexurally and torsionally simply supported.
- The most important results in the above plot, pertaining to the design of common metal building frame members, are the results for small values of P_u. One can observe that with the recommended calculations, the strengths at small P_u are represented very accurately.

7. Further Research

The updates provided in this paper show promise to remove significant conservatism in the Flange Local Buckling (FLB) and Tension Flange Yielding (TFY) provisions of the current AISC (2016) Specification in certain cases. The authors are in the process of investigating the results of these changes for a reasonably comprehensive range of member geometries in their on-going research, and final results from these studies are anticipated to appear in (Toğay, 2018).

One specific consideration under investigation is a minor interaction with the web shear strength in singly-symmetric members currently governed by TFY, where the flexural resistances can be

increased dramatically by "folding" the TFY considerations into the calculation of the yield moment to the compression flange, M_{cyT}. Moment-shear interaction considerations have been addressed extensively in the prior research by White et al. (2008), including experimental consideration of a wide range of hybrid cross-section members (lower web yield strength) with the neutral axis located at various depths including as extreme as being located within the compression flange at the strength limit. White et al. (2008) showed that moment-shear strength interaction could be neglected for a comprehensive range of I-section members. However, this was in the context of the current AISC (2016) TFY flexural resistance calculation as well as the shear buckling resistance for unstiffened webs and the AISC (2016) and AASHTO (2004) tension field shear resistance equations. The existing experimental results indicate that some minor moment-shear strength interaction needs to be considered in the broader context of the above recommended elimination of the AISC TFY resistance equations. Furthermore, when the shear postbuckling strength is considered for unstiffened webs, as implemented in the AISC (2016) Chapter G, some accounting for moment-shear strength interaction may be appropriate for extreme singly-symmetric sections where the tension flange exhibits early yielding. Subramanian (2017a) has conducted a limited number of studies of moment-shear interaction via test simulation. Her results indicate only minor interaction of the flexural and shear strengths. Therefore, it is believed that the above moment-shear strength interactions can be addressed by a simple reduction in the maximum calculated shear resistance in these cases.

8. Conclusion

This paper elucidates the conservatism of the current AISC (2016) Flange Local Buckling (FLB) and Tension Flange Yielding (TFY) resistance provisions in certain cases, recommends potential changes to the Specification that alleviate this issue, and provides detailed examples showing the improvement in the strength predictions by the recommended provisions. The recommended updates would significantly improve the quantification of beam and beam-column resistances in cases involving slender flanges in flexural compression as well as singly-symmetric members having a larger compression flange, such that the tension flange is subjected to early yielding.

Appendix

In this paper, test simulations are presented based on AISC (2016) Appendix 1.3, using residual stresses and geometric imperfections recommended by Subramanian and White (2017e). The details of these test simulation models are summarized below.

Finite Element Idealization

The ABAQUS 6.14 (Simulia 2014) finite element analysis software is employed to model the members considered in these study. In all cases, full nonlinear shell finite element solutions using the S4R element are used to model for both webs and flanges. The S4R is a four-node quadrilateral large strain shell formulation. The mesh is generated using 12 elements across the width of the flanges, and 20 elements through the depth of the web. The shell element aspect ratio is chosen to be approximately 1.0 in the web to determine the number of the elements along the member length.

Material Properties

The material properties F_y and E are multiplied by 0.9, as required by AISC 2016 Appendix 1.3. For the yield plateau of the material, the tangent stiffness is modeled as $E/1000$ for strains up to ten times the yield strain (ε_y). After this point, the strain hardening modulus is taken as $E/50$. At the levels of the strains observed in the test simulations, true stress versus log strain and engineering stress versus engineering strain are essentially the same.

Residual Stresses

Residual stresses of one-half the Best-fit Prawel pattern (Kim (2010)) for welded sections are assumed in all the studies (see Fig. 11). These residual stresses are recommended by Subramanian and White (2017e) as appropriate values necessary for close correlation with lateral torsional buckling experimental test results.
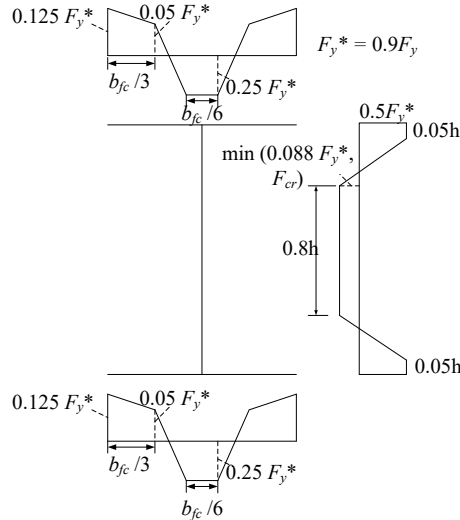
Figure 11: One-half of best-fit Prawel residual stress pattern for welded I-sections.

Geometric Imperfections

The test simulations include a base initial out-of-straightness of the flanges equal to one-half of the AWS (2010) and AISC Code of Standard Practice (COSP) geometric imperfection tolerance of $L_b/1000$, modified as discussed below. Subramanian and White (2017e) show that these reduced geometric imperfections are necessary for close correlation with experimental results.

Flange tilt and web out-of-flatness patterns are obtained by elastic eigenvalue buckling analysis of the members with the out-of-plane displacements restrained at the top and bottom flange-web juncture points, and with the members being subjected to uniform axial compression. Given the resulting buckling modes, the flange tilt and web-out-flatness are isolated and scaled to one-half the tolerance values as illustrated in Fig. 12.
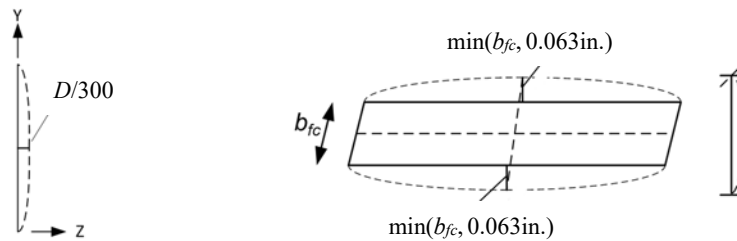
Figure 12.Web out-of-flatness and flange tilt imperfections.

The resulting flange tilt and web out-of-flatness imperfections are combined with a flange sweep that is applied at the web-flange juncture points. If the flange under consideration is subjected to flexural compression, a sinusoidal flange sweep is applied as shown in the top plot of Fig. 13. For the flange in flexural tension, zero sweep (i.e., an "Imperfection Factor" *IF* = 0) is applied if the net force in the flange is in tension. Otherwise a flange sweep between zero to $L_b/2000$ is applied based on *IF*. This is illustrated by the bottom plot in Fig. 13. The variation of *IF* as a function of

18

the ratio of the approximate axial forces in the flanges subjected to flexural tension and flexural compression, P_{ft}/P_{fc}, is shown in Fig. 14.

Flange Subjected to
Flexural Compression

$3L_b/8000$ $L_b/2000$ $3L_b/8000$

Flange Subjected to
Flexural Tension

$IF*$ $IF*$ $IF*$
$3L_b/8000$ $L_b/2000$ $3L_b/8000$
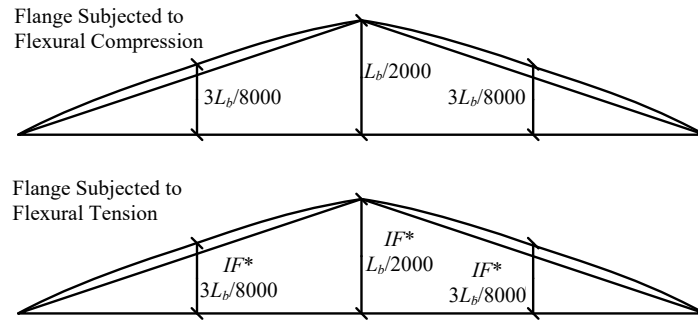
Figure 13. Applied sweep imperfections.

$$P_{ft} = \frac{M}{h_o} - \frac{P}{2}$$

$$P_{fc} = -\frac{M}{h_o} - \frac{P}{2}$$
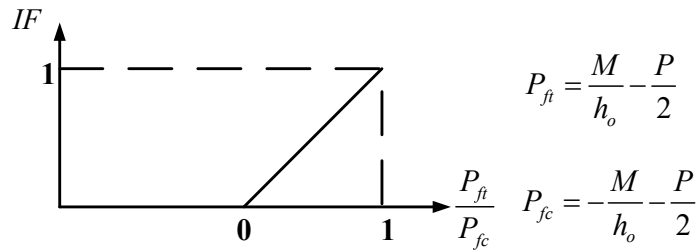
Figure 14. *IF* (tension flange sweep Imperfection Factor) calculation.

Acknowledgements

References

AASHTO (2017). *AASHTO LRFD Bridge Design Specifications. 8th Edition*, American Association of State Highway and Transportation Officials, Washington, DC.

AASHTO (2004). *AASHTO LRFD Bridge Design Specifications. 3th Edition*, American Association of State Highway and Transportation Officials, Washington, DC.

Abe, H., and Mizukoshi, N. (1973). "Buckling tests on plate girders under bending." *Annual Meeting of the Japanese Society of Civil Engineers, preprint*(Japan Society of Civil Engineers, Tokyo).

AISC (2005). *Specifications for Structural Steel Buildings, ANSI/AISC 360-05*, American Institute of Steel Construction, Chicago, IL.

AISC (2016). *Code of Standard Practice for Steel Buildings and Bridges, AISC 303-16*, American Institute of Steel Construction, Chicago, IL.

AISI (2012). *North American Specification for the Design of Cold-Formed Steel Structural Members*, ANSI/AISI S100-12, American Iron and Steel Institute, Washington, DC.

AISI (2016). *North American Specification for the Design of Cold-Formed Steel Structural Members*, ANSI/AISI S100-16, American Iron and Steel Institute, Washington, DC.

AWS (2010). *Structural Welding Code–Steel, AWS D1.1: D1.1M, 22nd ed*, AWS Committee on Structural Welding.

Carskaddan, P. S. (1968). "The bending behavior of slender-web girders with A514 steel flanges." *Applied Research, Rep. No. 57.019-904 (5) (AS-EA-23-ps), U.S. Steel Corporation, Pittsburgh.*

CEN (2005). *Design of Steel Structures, Part 1-1: General Rules and rules for buildings, EN 1993-1-1:2005:E, Incorporating Corrigendum February 2006*, European Committee for Standardization, Brussels, Belgium.

Holtz, N. M., and Kulak, G. L. (1973). "Web Slenderness Limits for Compact Beams." *Structural Engineering Report No 43.*, University of Alberta, Alberta, Canada, 41 pp.

Holtz, N. M., and Kulak, G. L. (1975). "Web Slenderness Limits for Non-compact Beams." *Structural Engineering Report No 51.*, University of Alberta, Alberta, Canada, 41 pp.

Greiner, R., and Kaim, P. (2001). "Comparison of LT-buckling design curves with test results." ECCS TC8, Rep. 23, European Convention for Constructional Steelwork, Zurich, Switzerland.

Janss, J., and Massonnet, C. (1967). "The Extension of Plastic Design to Steel A52." *Publications of the IABSE*, 27, 15-30.

Johnson, D. L. (1985). "An investigation into the interaction of flanges and webs in wide flange shapes." *Proc., Annual Technical Session, Structural Stability Research Council, U*Univ. of Missouri-Rolla, Rolla, Mo., 395–405.

Kim, Y. D. (2010). "Behavior and Design of Metal Building Frames Using General Prismatic and Web-Tapered Steel I-Section Members."Doctoral Dissertation, Georgia Institute of Technology, Atlanta, GA.

Lew, H. S., and Toprac, A. A. (1968). "The static strength of hybrid plate girders." *Structures Fatigue Research Laboratory, Dept. of Civil Engineering, Univ. of Texas, Austin, Texas*, S.F.R.L. Technical Rep. No. P550-11.

McDermott, J. F. (1969). "Plastic Bending of A514 Steel Beams." *Journal of the Structural Division, ASCE*, 95(9), 1851-1871.

Peköz, T. (1986). ''Development of a unified approach to the design of cold-formed steel members.'' Research Rep. No. CF 86-1, American Iron and Steel Institute, Washington, D.C.

Seif, M., and Schafer, B.W. (2009). "Finite Element Comparison of Design Methods for Locally Slender Steel Beams and Columns." *SSRC Annual Stability Conference*Phoenix, AZ. .

Simulia (2014). *ABAQUS/Standard Version 6.14-2*, Simulia, Inc, Providence, RI.

Subramanian, L. P., Jeong, W. Y., Yellepeddi, R., and White, D. W. (2018). "Assessment of I-Section Member LTB Resistances Considering Experimental Test Data." *Engineering Journal*, 55, 15-44.

Subramanian, L. P., and White, D. W. (2017a). "Flexural Resistance of Longitudinally Stiffened Plate Girders." *Updated Report to AASHTO and AISI,* School of Civil and Environmental Engineering, Georgia Institute of Technology, January, 392 pp

Subramanian, L. P., and White, D. W. (2017b). "Improved Noncompact Web-Slenderness Limit for Steel I-Girders" *Journal of Structural Engineering*, ASCE, 143(4).

Subramanian, L. and White, D.W. (2017c). "A Reassessment of the Lateral Torsional Buckling Resistance of I-Section Members – Uniform Moment Studies," *Journal of Structural Engineering*, ASCE, 143(3).

Subramanian, L. and White, D.W. (2017d). "A Reassessment of the Lateral Torsional Buckling Resistance of Rolled I-Section Members – Moment Gradient Tests," Journal of Structural Engineering, ASCE, 143(4).

Subramanian, L. P., and White, D. W. (2017e). "Resolving the disconnects between lateral torsional buckling experimental tests, test simulations and design strength equations." *Journal of Constructional Steel Research*, 128, 321-334..

Toğay, O., and White, D. W. (2017). "Comprehensive Stability Design of Steel Members and Systems via Inelastic Buckling Analysis – Beam-Column Validation Studies." *Proceedings of the Annual Stability Conference Structural Stability Research Council*San Antonio, TX.

Toğay, O. (2018). "Comprehensive Stability Design of Steel Members and Systems via Inelastic Buckling Analysis" Ph.D. dissertation, School of Civil and Environmental Engineering, Georgia Institute of Technology, Atlanta (to appear).

White, D. W. (2008). "Unified flexural resistance equations for stability design of steel I-section members: Overview." *Journal of Structural Engineering-American Society of Civil Engineers*, 134(9), 1405-1424.

White, D.W., Barker, M. and Azizinamini, A. (2008). "Shear Strength and Moment-Shear Interaction in Transversely-Stiffened Steel I-Girders," *Journal of Structural Engineering*, ASCE, 134(9), 1437-1449.

White, D. W., Jeong, W. Y., and Toğay, O. (2016). "Comprehensive stability design of planar steel members and framing systems via inelastic buckling analysis." *International Journal of Steel Structures*, 16(4), 1029-1042.

White, D. W., and Kim, Y. D. (2008). "Unified Flexural Resistance Equations for Stability Design of Steel I-Section Members: Moment Gradient Tests." *Journal of Structural Engineering*, 134(9), 1471-1486.